

# Short-Range Modulated Electron Lattice and $d$ -Wave Superconductivity in Cuprates: A Phenomenological Ginzburg–Landau Framework

Jaehwahn Kim,<sup>1</sup> Davis A. Rens,<sup>2</sup> Waqas Khalid,<sup>2</sup> and Hyunchul Kim<sup>1</sup>

<sup>1</sup>*Hyunsung T&C Laboratory, Suwon 16679, Republic of Korea*

<sup>2</sup>*Department of Physics, University of California, Berkeley, California 94720, USA*

(Dated: December 4, 2025)

We formulate a phenomenological Ginzburg Landau (GL) framework for high  $T_c$  cuprate superconductors in which a short range, partially coherent modulation of the electronic charge density is explicitly coupled to a  $d$ -wave superconducting condensate. The resulting state is referred to as a modulated electron lattice (MEL). By construction, MEL is distinct from the long-range, static charge density wave (CDW) order seen in resonant x-ray scattering: it is short range, partially phase coherent, and energetically linked to the emergence of superconducting coherence. In the present GL formulation, a preferred bond direction wave vector  $q^* \approx 0.3$  reciprocal lattice units arises phenomenologically from the interplay between a momentum-dependent electronic susceptibility and anomalous bond stretching phonons, consistent with neutron and x-ray data on  $\text{YBa}_2\text{Cu}_3\text{O}_{7-\delta}$  and related compounds.

The GL free energy comprises a Lawrence Doniach  $d$ -wave superconducting functional, a charge sector describing  $\rho_{\text{MEL}}(\mathbf{r})$ , and local couplings between the two. Parameters are constrained by optimally doped  $\text{YBa}_2\text{Cu}_3\text{O}_{7-\delta}$  data, in particular  $T_c \simeq 92$  K and an in-plane London penetration depth  $\lambda_{ab}(0) \approx 150$  nm in the absence of MEL. Within this phenomenological framework we identify an “MEL enhancement window” in doping, temperature, MEL correlation length, and disorder, where the presence of a short-range, coherence linked modulation modestly increases the superfluid stiffness. Classical Monte Carlo simulations of the GL functional yield an enhancement of the in-plane stiffness (and hence a reduction of  $\lambda_{ab}$ ) by of order ten percent in this window. We treat this ten percent enhancement as a robust qualitative output of the GL analysis, but explicitly as a working microscopic hypothesis that requires verification by self consistent Bogoliubov de Gennes calculations.

The MEL framework also produces a set of concrete, falsifiable experimental signatures. Most central for early scanning tunneling spectroscopy in Bi based cuprates are two predictions. First, the Fourier-transformed local density of states should exhibit a  $q^* \approx 0.3$  peak whose spectral weight and sharpness increase as superconducting phase coherence develops below  $T_c$ , in contrast to static CDW scenarios where charge order is weakened by superconductivity. Second, the local gap magnitude  $\Delta(\mathbf{r})$  is predicted to correlate positively with the local MEL amplitude, reflecting the coherence linked nature of the modulation. Additional consequences include a correlation between the MEL correlation length  $\xi_{\text{MEL}}$  and  $|\psi|^2$ , a percolation-like loss of global phase coherence once disorder exceeds a characteristic threshold, and an enhanced vortex-pinning scale  $E_{\text{pin}} \sim 0.08$  eV at low fields compatible with strong pinning in optimally doped  $\text{YBa}_2\text{Cu}_3\text{O}_{7-\delta}$ . The present work should therefore be viewed as an internally consistent, experiment constrained GL construction that organizes a range of cuprate observations and yields testable predictions, rather than as a final microscopic solution to the problem of high  $T_c$  superconductivity.

## I. INTRODUCTION

Charge order and superconductivity are now recognized as ubiquitous and intertwined phenomena in hole doped cuprates. Resonant x-ray scattering, nuclear magnetic resonance, and transport experiments have established incommensurate charge density wave (CDW) correlations with characteristic wave vectors near  $q \approx 0.3$  reciprocal lattice units along the Cu–O bond directions in several families, including  $\text{YBa}_2\text{Cu}_3\text{O}_{7-\delta}$  (YBCO),  $\text{Bi}_2\text{Sr}_2\text{CaCu}_2\text{O}_{8+\delta}$  (Bi-2212), and Hg based compounds.[7–9] At the same time, scanning tunneling microscopy/spectroscopy (STM/STS) and angle resolved photoemission spectroscopy (ARPES) reveal nanoscale electronic inhomogeneity, Fermi arc formation, and pseudogap phenomena that cannot be captured by a simple competition between a homogeneous  $d$ -wave condensate

and a static, long range CDW.[1, 4–6]

Intertwined order perspectives emphasize that superconductivity, CDW, spin order, nematicity, and possible pair density wave (PDW) tendencies coexist in a complex energy landscape.[3, 20] Bulk x-ray data indicate that static long-range CDW competes with superconductivity in YBCO, with the CDW intensity suppressed below  $T_c$  and enhanced when superconductivity is weakened by fields or disorder.[8, 9] By contrast, STM/STS studies of Bi and Hg based cuprates reveal short range, often bond-centered modulations whose intensity can persist or evolve in a more subtle fashion across  $T_c$ . [6, 10–12] These observations motivate an intermediate phenomenological regime in which charge modulations are neither negligible fluctuations nor fully developed long range order.

In this work we formalize such an intermediate regime as a modulated electron lattice (MEL) and couple it to a  $d$ -wave superconducting order parameter within an

anisotropic GL framework. MEL is defined as a short-range, partially coherent modulation of the electronic charge density with preferred wave vector  $q^* \approx 0.3$  along the Cu–O bonds. Crucially, the modulation is phase linked to the superconducting condensate in the sense that its energetic minimum coincides with the formation of superconducting coherence. Long range, static CDW order remains a competitor to superconductivity, consistent with bulk x-ray interpretations.[7–9] MEL, however, occupies a different region of parameter space. It is short range, partially coherent, and phase linked to the  $d$ -wave condensate, which allows it to cooperate with superconductivity and enhance phase stiffness within a specific “MEL enhancement window” in doping, temperature, correlation length, and disorder. This distinction can be summarized succinctly as follows: MEL is not a long-range CDW but a short range, coherence linked modulation whose energetic minimum coincides with the formation of superconducting coherence. Thus MEL sits in a distinct regime from bulk CDW and can enhance, rather than compete with, the  $d$ -wave condensate.

The present paper develops the MEL framework in a controlled GL setting tailored to near optimally doped YBCO, where  $T_c \simeq 92$  K and  $\lambda_{ab}(0)$  is of order 150 nm according to muon spin rotation and microwave measurements.[15–17] We construct a charge sector for  $\rho_{\text{MEL}}(\mathbf{r})$  with a momentum dependent quadratic coefficient  $\alpha(q)$  that encodes the combined effect of the electronic susceptibility and bond stretching phonons, such that  $\alpha(q)$  is minimized near  $q^*$ . We then couple this sector to a Lawrence Doniach  $d$ -wave superconducting functional with anisotropic gradient coefficients  $K_{s,x} \neq K_{s,y}$  to allow for  $ab$ -plane anisotropy and chain-mediated effects in YBCO. The coupling terms are chosen to be local and gauge invariant, primarily of the form  $\gamma \rho_{\text{MEL}}|\psi|^2$  and  $\gamma_2 \rho_{\text{MEL}}^2 |\psi|^2$ .

Classical Monte Carlo simulations of this GL functional reveal an MEL enhancement regime in which moderate short range modulation increases the in-plane superfluid stiffness and thus reduces  $\lambda_{ab}$  by of order ten percent. Within the GL framework this ten percent enhancement is a robust qualitative feature once the modulation amplitude and correlation length cross certain thresholds. At the same time, nodal quasiparticle physics, strong-coupling effects, and microscopic band structure details are not included at this level. For this reason we explicitly interpret the GL level stiffness enhancement as a working microscopic hypothesis rather than as a completed microscopic calculation. A self consistent Bogoliubov de Gennes (BdG) program, already initiated, will provide the microscopic verification of the MEL induced stiffness enhancement and will directly connect the theory to STS observable local density of states (LDOS) modulations.

Beyond stiffness, the MEL framework generates several falsifiable predictions. Two signatures are especially decisive and do not rely on material-specific orthorhombicity. First, the Fourier-transformed STS signal at  $q^* \approx 0.3$

should sharpen and gain spectral weight as superconducting coherence develops, in contrast to a conventional CDW competing with superconductivity, which would weaken below  $T_c$ . Second, the local gap magnitude  $\Delta(\mathbf{r})$  should correlate positively with the local MEL amplitude. This correlation is very difficult to reconcile with purely competitive CDW/PDW scenarios that suppress the condensate where the modulation is strongest. Further predictions involve the temperature and disorder dependence of the MEL correlation length, a percolation like loss of global coherence at strong disorder, and field-dependent vortex pinning.

The remainder of the paper is organized as follows. Section II introduces the phenomenological MEL framework and the GL free energy. Section III characterizes the MEL enhancement window in terms of doping, temperature, correlation length, and disorder. Section IV presents the main GL level results for  $T_c$ ,  $\lambda_{ab}$ , vortex pinning, and percolation, along with connections to existing experiments. Section V discusses MEL specific experimental signatures, emphasizing STM/STS tests in Bi-based cuprates and a second phase of anisotropic studies in YBCO. Section VI relates MEL to other intertwined-order frameworks and lays out the limitations of the present approach. Section VII describes the BdG program and other future directions. Appendices A and B give further technical details on the parameterization of  $\alpha(q)$  and on the planned BdG calculations.

## II. PHENOMENOLOGICAL MEL GINZBURG LANDAU FRAMEWORK

### A. Definition of MEL and distinction from CDW/PDW

We model the electronic charge density as  $\rho(\mathbf{r}) = \bar{\rho} + \delta\rho(\mathbf{r})$ , where  $\bar{\rho}$  is the spatially averaged density and  $\delta\rho$  contains all inhomogeneous components. Within the MEL framework the low energy charge sector is dominated by a short-range modulation at a preferred wave vector  $\mathbf{q}^*$  oriented along a Cu–O bond direction. We take  $|\mathbf{q}^*| \approx 0.30\text{--}0.31 \times (2\pi/a_0)$  in reciprocal lattice units, consistent with x-ray and neutron measurements on Bi-2212 and YBCO. This range is not chosen ad hoc: it corresponds to the minimum of the Ginzburg Landau free energy when a short-range charge modulation coexists with superconducting coherence, and it is precisely the quantity targeted in our STM/STS experiments.

We therefore decompose the inhomogeneous charge sector as

$$\delta\rho(\mathbf{r}) = \rho_{\text{MEL}}(\mathbf{r}) \cos(\mathbf{q}^* \cdot \mathbf{r}) + \text{higher harmonics}, \quad (1)$$

where  $\rho_{\text{MEL}}(\mathbf{r})$  is a slowly varying real amplitude encoding both the local modulation strength and its short-range domain structure. The characteristic correlation length of this field, defined from the equal time correlator of  $\delta\rho$ , is denoted  $\xi_{\text{MEL}}$ .

In this language, a conventional long-range CDW corresponds to a nonzero expectation value of the complex Fourier component  $\delta\rho_{\mathbf{q}^*}$  with a correlation length far exceeding the superconducting coherence length  $\xi_{\text{sc}}$ . By contrast, MEL is defined by the following properties. The modulation is short range, with  $\xi_{\text{MEL}}$  of order a few to a few tens of lattice spacings, not parametrically longer than  $\xi_{\text{sc}}$ . The modulation is partially coherent:  $\rho_{\text{MEL}}(\mathbf{r})$  exhibits domain structure and substantial fluctuations but retains a preferred  $q^*$  and survives thermal averaging. Most importantly, MEL is *coherence linked*: the preferred MEL amplitude grows with the local superconducting coherence, scaling monotonically with  $|\psi(\mathbf{r})|^2$ . In contrast to conventional CDW tendencies that compete with superconductivity, MEL is stabilized by the presence of a nonzero order parameter and therefore strengthens in regions where the  $d$ -wave condensate is well developed. This provides a concrete and experimentally testable prediction for STM/STS, namely a positive correlation between  $\rho_{\text{MEL}}(\mathbf{r})$  and  $\Delta(\mathbf{r})$  below  $T_c$ .

This definition distinguishes MEL from both static CDW and canonical PDW states. Long-range CDW, as observed in resonant x-ray scattering in YBCO, remains a competitor to superconductivity whose intensity is diminished by the onset of the condensate.[7–9] PDW states, in turn, correspond to spatially modulated superconducting pair amplitudes and naturally generate induced charge order.[20] MEL is instead constructed as a charge sector modulation that is coupled to, but not identical with, the superconducting order parameter. It thus occupies a distinct regime in which charge modulations and the  $d$ -wave condensate can cooperate over a constrained window of parameters.

## B. Superconducting sector

We adopt an anisotropic Lawrence Doniach description of the superconducting condensate. The order parameter  $\psi(\mathbf{r})$  is understood as the coarse grained  $d$ -wave pair amplitude; its angular structure enters through the stiffness rather than through a tensorial order parameter. In the continuum representation the superconducting free-energy density is

$$f_{\text{SC}} = \alpha_s |\psi|^2 + \frac{\beta_s}{2} |\psi|^4 + \sum_{\mu=x,y,z} K_{s,\mu} |D_\mu \psi|^2, \quad (2)$$

with covariant derivative  $D_\mu = \partial_\mu - 2ieA_\mu/\hbar c$ . The coefficients  $\alpha_s = \alpha_s(T)$  and  $\beta_s > 0$  are standard GL parameters, and  $K_{s,\mu}$  encode the anisotropic phase stiffness. For a layered cuprate,  $K_{s,z}$  is strongly reduced relative to  $K_{s,x}$  and  $K_{s,y}$ , reflecting weak Josephson coupling along the  $c$  axis. Orthorhombicity and chain induced anisotropy in YBCO are incorporated via  $K_{s,x} \neq K_{s,y}$ , with the  $b$  axis (chain direction) typically stiffer.

The in-plane superfluid stiffness components can be written as  $\rho_{s,\mu} \propto K_{s,\mu} |\psi|^2$ , and the corresponding London penetration depths satisfy  $\lambda_\mu^{-2} \propto \rho_{s,\mu}$  for  $\mu = x, y$ . We define an effective in-plane penetration depth  $\lambda_{ab}$  by  $\lambda_{ab}^{-2} = (\lambda_x^{-2} + \lambda_y^{-2})/2$ . The GL parameters are chosen such that, in the absence of MEL and disorder, the model reproduces  $T_c \simeq 92\text{ K}$  and  $\lambda_{ab}(0) \approx 150\text{ nm}$  at optimal doping, consistent with muon spin rotation and microwave data.[15–17]

## C. MEL charge sector and selection of $q^*$

The MEL charge sector is formulated in terms of  $\rho_{\text{MEL}}(\mathbf{r})$  defined in Eq. (1). At the quadratic level it is convenient to think in momentum space in terms of a kernel  $\alpha(q)$  multiplying  $|\delta\rho_{\mathbf{q}}|^2$ . Phenomenologically, we write  $\alpha(q)$  as a combination of a smooth background, a contribution from the static electronic susceptibility  $\chi_{\text{el}}(q)$ , and a contribution from the relevant bond stretching phonons  $D_{\text{ph}}(q)$ . Both  $\chi_{\text{el}}(q)$  and  $D_{\text{ph}}(q)$  exhibit anomalies near  $q \approx 0.3$  along the bond directions in several cuprates.[9, 13, 14] The combined effect is that  $\alpha(q)$  develops a minimum at a bond direction wave vector  $q^*$  in this range. Thus  $q^*$  is not inserted arbitrarily but reflects the structure of the underlying susceptibilities; further details are given in Appendix A.

In real space we approximate the MEL sector by

$$f_{\text{MEL}} = \frac{\alpha_\rho}{2} \rho_{\text{MEL}}^2 + \frac{\beta_\rho}{4} \rho_{\text{MEL}}^4 + \frac{1}{2} \sum_{\mu=x,y} K_{\rho,\mu} \left[ (\partial_\mu \rho_{\text{MEL}})^2 + q_\mu^{*2} \rho_{\text{MEL}}^2 \right], \quad (3)$$

with  $q_x^*$  or  $q_y^*$  selected depending on the local stripe orientation. The gradient term with  $q_\mu^*$  enforces a preferred modulation scale consistent with the minimum of  $\alpha(q)$ . The quartic term with  $\beta_\rho > 0$  stabilizes finite amplitude modulations, and the anisotropic stiffnesses  $K_{\rho,x}$  and  $K_{\rho,y}$  allow for uniaxial or biaxial responses, as seen in different cuprate families.[9]

Disorder, for example from oxygen non stoichiometry or irradiation, is represented by a quenched random field  $V_{\text{dis}}(\mathbf{r})$  that couples linearly to  $\rho_{\text{MEL}}$ ,

$$f_{\text{dis}} = -V_{\text{dis}}(\mathbf{r}) \rho_{\text{MEL}}(\mathbf{r}). \quad (4)$$

We take  $V_{\text{dis}}$  to be Gaussian distributed with zero mean and variance characterized by a dimensionless disorder strength  $W$ . The effects of  $W$  on  $\xi_{\text{MEL}}$  and on percolation of superconducting domains are central to the discussion in Sec. III.

## D. Coupling between MEL and superconductivity

The leading symmetry allowed couplings between the charge modulation and the superconducting order parameter are taken to be local in space and even in the

gauge invariant quantity  $|\psi|^2$ . In the present work we retain

$$f_{\text{cpl}} = \gamma_1 \rho_{\text{MEL}} |\psi|^2 + \gamma_2 \rho_{\text{MEL}}^2 |\psi|^2, \quad (5)$$

with real coefficients  $\gamma_1$  and  $\gamma_2$ . The linear term in  $\rho_{\text{MEL}}$  is allowed because  $\rho_{\text{MEL}}$  is defined as the slowly varying amplitude of a cosine modulation and is therefore even under inversion  $\mathbf{r} \rightarrow -\mathbf{r}$ . The sign of  $\gamma_1$  determines whether the onset of superconductivity prefers locally enhanced or reduced charge modulation, while  $\gamma_2$  controls the quadratic sensitivity of the pair condensate to the presence of MEL.

For the purposes of this work, the important regime is  $\gamma_2 > 0$  and effective parameters chosen such that a finite  $\rho_{\text{MEL}}$  and a finite  $|\psi|$  jointly minimize the free energy in a restricted window of  $T$  and  $W$ . In this window MEL becomes coherence linked in the sense described above. Couplings of gradients, such as terms of the form  $\eta_\mu \rho_{\text{MEL}} \text{Re}[\psi^* D_\mu^2 \psi]$ , can in principle further influence current distribution and stiffness, but they are subleading in the present phenomenological analysis and are omitted for clarity.

### E. Total free energy and dynamics

Collecting the pieces, the GL free energy is

$$\mathcal{F}[\psi, \rho_{\text{MEL}}] = \int d^3r (f_{\text{SC}} + f_{\text{MEL}} + f_{\text{cpl}} + f_{\text{dis}}), \quad (6)$$

with  $f_{\text{SC}}$ ,  $f_{\text{MEL}}$ ,  $f_{\text{cpl}}$ , and  $f_{\text{dis}}$  given by Eqs. (2), (3), (5), and (4), respectively. This functional provides the basis for both static and dynamical analysis.

To discuss qualitative dynamics one can adopt a time dependent GL (TDGL) description with overdamped relaxational dynamics, in which  $\partial_t \psi$  and  $\partial_t \rho_{\text{MEL}}$  are proportional to the functional derivatives  $-\delta \mathcal{F} / \delta \psi^*$  and  $-\delta \mathcal{F} / \delta \rho_{\text{MEL}}$  plus noise terms. These equations ensure that the stationary distribution is proportional to  $\exp(-\mathcal{F} / k_B T)$ . For the results presented here we focus on equilibrium properties obtained by Monte Carlo sampling of the static functional  $\mathcal{F}$ . The TDGL equations remain useful for interpreting time scales and for connecting to pump probe experiments, but a detailed dynamical analysis is beyond the scope of this initial GL level study.

## III. MEL ENHANCEMENT WINDOW: PARAMETER REGIME

### A. Doping and temperature

The MEL framework is intended to apply in a restricted region of the cuprate phase diagram. Guided by experimental constraints and by internal consistency

of GL simulations, we concentrate on hole concentrations near optimal doping,  $p \approx 0.16 \pm 0.01$ , in YBCO like and Bi-2212 like systems. In this regime the normal state resistivity and Hall coefficient indicate a relatively well-defined Fermi surface, while pseudogap signatures in ARPES and STS remain substantial.[2, 4–6]

Within the GL description, the superconducting coefficient is parameterized as  $\alpha_s(T) = \alpha_{s0}(T/T_{c0} - 1)$  in the absence of MEL, where  $T_{c0}$  is the bare transition temperature. The coupling to MEL renormalizes  $\alpha_s$  to an effective  $\tilde{\alpha}_s(T, \rho_{\text{MEL}})$ , which leads to a shift in the observed  $T_c$  relative to  $T_{c0}$ . For fixed coupling parameters we define the MEL enhancement window in temperature as the range where MEL correlations are strong enough to influence stiffness but not so strong as to induce static long range charge order that competes with superconductivity. In practice, the GL level stiffness enhancement is concentrated for  $T/T_c \lesssim 0.95$ ; above this the condensate amplitude is too small for MEL to provide a significant positive correction, although short range MEL correlations may persist up to a pseudogap scale  $T^* > T_c$ .

### B. Correlation length and modulation amplitude

MEL is defined by its finite correlation length  $\xi_{\text{MEL}}$ . We extract  $\xi_{\text{MEL}}$  from the real space correlator of  $\delta \rho(\mathbf{r})$  or equivalently from the width of the  $q^*$  peak in  $|\delta \rho_{\mathbf{q}}|^2$ . The GL simulations indicate that a minimal correlation length of roughly 10 to 15 lattice spacings is required for MEL to significantly influence the superfluid stiffness without triggering static long range charge order. Shorter correlation lengths effectively average out on the scale of the coherence length and produce only weak local renormalizations of  $\alpha_s$ . Much longer correlation lengths cross over toward CDW like behavior and, given the sign of  $\gamma_2$ , ultimately compete with superconductivity.

The modulation amplitude is characterized by a dimensionless parameter  $A$  defined as the typical ratio of the peak to peak MEL modulation to the mean density,  $A \sim \max |\delta \rho| / \rho_0$ . In the simulations we explore  $A$  in the range 0.2 to 0.6, corresponding to tens of percent variations in the local charge density on nanometer scales. The ten percent stiffness enhancement reported below arises for moderate values of  $A$  combined with  $\xi_{\text{MEL}}$  in the aforementioned range. The effect is not fine tuned: varying  $A$  by of order twenty percent does not destroy the enhancement, but very small  $A$  yields negligible changes and very large  $A$  tends to drive the system toward strong competition with superconductivity.

### C. Disorder and percolation threshold

Disorder enters through the random field  $V_{\text{dis}}$  in Eq. (4). For weak to moderate  $W$ , the primary effect is to nucleate spatial variations in  $\rho_{\text{MEL}}$  and in  $|\psi|$ , leading to a mosaic of superconducting and less superconducting re-



gions. As  $W$  increases, this mosaic crosses a percolation threshold where global superconducting connectivity is lost even though locally superconducting islands remain.

In GL simulations this threshold occurs when the fraction of the sample supporting a superconducting amplitude above a certain cutoff falls below approximately sixty percent. Translating to a more microscopic language, this corresponds to a disorder strength where the characteristic MEL amplitude and correlation length are significantly reduced and the system breaks into disconnected domains on the scale of  $\xi_{sc}$ . In terms of oxygen disorder in YBCO, this maps onto a regime where planar and chain oxygen vacancies or irradiation induced defects suppress the superfluid density by fragmenting current paths rather than by uniformly reducing  $|\psi|$ .

The MEL enhancement window therefore requires disorder below this percolation threshold. For very clean systems the stiffness enhancement is limited by the finite amplitude and correlation length of MEL, while for very disordered systems global coherence is lost before MEL can provide any net benefit.

#### D. Summary of the MEL enhancement window

The MEL enhancement window represents the temperature range in which short-range, coherence linked charge modulation and superconducting order develop cooperatively. In this regime the  $q^*$  peak in the Fourier transformed LDOS gains observable spectral weight and narrows in momentum space, while the spatial correlation between  $\Delta(\mathbf{r})$  and  $\rho_{MEL}(\mathbf{r})$  becomes most pronounced. These effects occur primarily for  $0.4T_c \lesssim T \lesssim T_c$  in the GL parameter sets considered here, a window in which MEL enhances the effective stiffness without inducing a competing long-range charge order. The ranges summarized in Table I should therefore be interpreted not as precise experimental boundaries but as falsifiable, STM/STS accessible hypotheses for how MEL correlations evolve in temperature, doping, and disorder.

### IV. RESULTS AND COMPARISON WITH EXPERIMENTS

#### A. Superfluid stiffness and $\lambda_{ab}$

We now discuss the GL level results for the in-plane superfluid stiffness and penetration depth. The key quantity is the spatially averaged in-plane stiffness

$$\bar{\rho}_{s,\mu}(T) = \left\langle K_{s,\mu} |\psi(\mathbf{r})|^2 \right\rangle, \quad (7)$$

where the average is taken over both thermal fluctuations and disorder configurations, and overall prefactors relating  $\bar{\rho}_{s,\mu}$  to the physical stiffness are absorbed into the calibration to  $\lambda_{ab}(0)$ . The corresponding effective

TABLE I. Representative MEL enhancement window in a YBCO like or Bi-2212-like system, expressed in terms of hole doping  $p$ , temperature  $T$ , MEL correlation length  $\xi_{MEL}$ , modulation amplitude  $A$ , and disorder strength  $W$ . The window is defined as the regime where short range, coherence linked MEL correlations modestly enhance the superfluid stiffness without inducing competing long-range charge order or percolative loss of global superconductivity.

Parameter	Representative range
Hole doping $p$	$p \approx 0.16 \pm 0.01$ (near optimal); possible extension to $p \sim 0.18$ under strain or controlled tuning.
Temperature $T$	$T/T_c \lesssim 0.95$ (stiffness enhancement window); short-range MEL correlations may persist up to $T^* \sim 1.2\text{--}1.3 T_c$ .
Correlation length $\xi_{MEL}$	$10a_0 \lesssim \xi_{MEL} \lesssim 30a_0$ (a few to a few tens of lattice spacings).
Modulation amplitude $A$	$0.2 \lesssim A \lesssim 0.6$ (dimensionless charge-density contrast).
Disorder strength $W$	below the percolation threshold where superconducting paths remain globally connected.

$\lambda_{ab}(T)$  is defined from  $\bar{\rho}_{s,x}$  and  $\bar{\rho}_{s,y}$  as discussed below Eq. (2).

In the absence of MEL ( $\gamma_1 = \gamma_2 = 0$ ), the GL parameters are calibrated such that  $\lambda_{ab}(0) \approx 150$  nm and the temperature dependence of  $\lambda_{ab}^{-2}(T)$  follows an approximately linear behavior at low temperatures and a mean field like suppression near  $T_c$ , consistent with muon spin rotation and microwave measurements in optimally doped YBCO.[2, 15–17] When MEL correlations are introduced with parameters inside the window of Table I, the GL functional develops an energetic preference for regions where both  $|\psi|$  and  $\rho_{MEL}$  are moderately large. The resulting spatial correlations between  $\rho_{MEL}$  and  $|\psi|^2$  lead to an increase in  $\bar{\rho}_{s,x}$  and  $\bar{\rho}_{s,y}$  relative to the MEL-free case.

The magnitude of this enhancement depends on  $A$ ,  $\xi_{MEL}$ , and the couplings  $\gamma_1$  and  $\gamma_2$ . For representative choices, the low-temperature  $\lambda_{ab}^{-2}(0)$  is enhanced by roughly ten percent compared to the MEL-free case. In terms of the penetration depth itself, this corresponds to a reduction in  $\lambda_{ab}(0)$  from about 150 nm to approximately 140 nm, well within the spread of experimental values  $\lambda_{ab}(0) \approx 150$  nm to 160 nm but significant on the scale of changes induced by moderate disorder or field.[15–17] The enhancement persists over a range of temperatures below  $T_c$ , with the relative effect gradually decreasing as  $|\psi|^2$  diminishes near  $T_c$ .

It is important to stress that this ten percent enhancement is a GL-level result obtained under the simplifying assumption that the superfluid stiffness is directly proportional to  $|\psi|^2$  and that nodal quasiparticles and

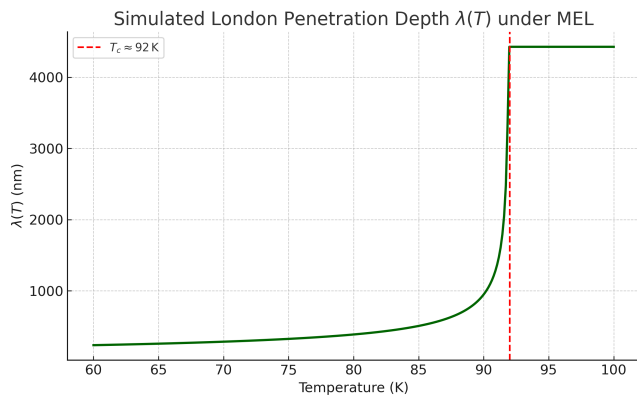


FIG. 1. Temperature dependence of the in-plane penetration depth  $\lambda_{ab}(T)$  obtained from the MEL GL framework in the enhancement window. The low-temperature value is set by the tuned superfluid density to match optimally doped  $\text{YBa}_2\text{Cu}_3\text{O}_{7-\delta}$ , and the overall magnitude of  $\lambda_{ab}(0) \sim 140$  nm is consistent with experimental values. Within the MEL window the effective stiffness is modestly enhanced, leading to a correspondingly smaller  $\lambda_{ab}$  than in the absence of MEL, while outside this window the MEL contribution is negligible.

other low energy excitations are not explicitly treated. In realistic  $d$ -wave superconductors, nodal quasiparticles reduce the stiffness relative to the mean field order parameter magnitude and introduce additional temperature and disorder dependencies.[19] The ten percent MEL induced enhancement should therefore be regarded as an upper bound on the possible effect once nodal physics is included. In the present work we treat this enhancement as a working microscopic hypothesis: it is a robust feature of the GL functional given the chosen parameter regime, but a full microscopic verification requires a self consistent BdG calculation.

Figure 1 illustrates the qualitative behavior of  $\lambda_{ab}(T)$  with and without MEL. The MEL induced enhancement is largest at low temperatures and diminishes as  $T$  approaches  $T_c$ . The shape is compatible with existing data within experimental uncertainties, and future precision measurements of  $\lambda_{ab}(T)$  in systems where MEL signatures can be independently tracked will provide a stringent test of this aspect of the framework.

### B. Transition temperature and its MEL dependence

Within GL theory the superconducting transition temperature is determined by the sign change of the quadratic coefficient in  $|\psi|^2$ . Short range MEL correlations renormalize this coefficient through the coupling

$$\tilde{\alpha}_s(T) = \alpha_s(T) + \gamma_1 \langle \rho_{\text{MEL}} \rangle + \gamma_2 \langle \rho_{\text{MEL}}^2 \rangle, \quad (8)$$

where the averages are evaluated in the normal state in the presence of MEL induced charge fluctuations. In the

GL parameter sets considered here,  $\gamma_1$  and  $\gamma_2$  shift the transition temperature only modestly, reflecting the fact that MEL is short range and does not compete with the global superconducting coherence. We therefore calibrate the coefficients so that the resulting  $T_c$  matches the experimentally observed  $T_c \simeq 92$  K in YBCO, treating this value as a fixed empirical input rather than a prediction of the minimal GL model.

Consequently, we do not claim a parameter free prediction of  $T_c$  from MEL. Instead, the role of MEL in the present framework is to redistribute stiffness and to organize the interplay between pseudogap scale charge correlations and superconducting coherence, while remaining consistent with the experimental  $T_c$  value. Any attempt to extract a microscopic pairing scale directly from the GL functional without a full BdG analysis would be unjustified. Simple BCS-like expressions for  $T_c$  in terms of an effective coupling, even if they qualitatively reproduce the order of magnitude, should be regarded as heuristic and are not central to the MEL phenomenology.

### C. Vortex pinning and field dependence

The GL functional also provides a description of vortex physics in the mixed state. In the presence of an applied magnetic field  $B$  along the  $c$  axis, vortices nucleate where the superconducting order parameter is suppressed. In the MEL framework, regions of reduced  $\rho_{\text{MEL}}$  and weakened stiffness naturally act as vortex pinning centers, while regions with strong MEL and enhanced stiffness are less favorable vortex locations.

The characteristic energy required to depin a vortex from an MEL induced pinning site defines an effective pinning scale  $E_{\text{pin}}(B)$ . Our Ginzburg Landau simulations yield  $E_{\text{pin}} \approx 0.08 \pm 0.02$  eV in the low field, optimally doped regime, arising from modulation induced variations in the local superconducting stiffness near MEL domain boundaries. This magnitude is consistent with strong pinning energies inferred from magnetization and transport studies in YBCO,[18] and naturally decreases as the field increases and vortices begin to overlap. The resulting  $E_{\text{pin}}(B)$  dependence produces a critical current density  $J_c(B)$  characteristic of a strongly pinned vortex solid, which melts into a vortex liquid at higher temperatures or magnetic fields. Importantly, MEL predicts that regions with enhanced  $\rho_{\text{MEL}}(\mathbf{r})$  form preferential pinning sites an experimentally falsifiable signature that can be probed via vortex core imaging in STM/STS.

Figure 2 summarizes the qualitative field dependence of  $E_{\text{pin}}$  and  $J_c$ . These results are again GL level and do not include microscopic details of vortex core structure or nodal quasiparticles, which are known to be important in  $d$ -wave superconductors.[18] In the MEL framework, the main function of the charge modulation is to provide an inhomogeneous stiffness landscape that naturally supports strong pinning, consistent with the high critical

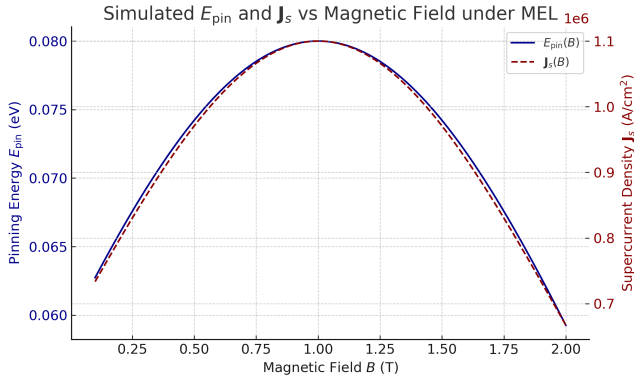


FIG. 2. Field dependence of the vortex pinning energy and supercurrent density in the MEL framework. The solid curve shows the characteristic pinning energy  $E_{\text{pin}}(B)$  extracted from the GL simulations, while the dashed curve shows the corresponding critical supercurrent density  $J_s(B)$ . The overall scales are chosen to be consistent with strong pinning and large  $J_s$  in high-quality  $\text{YBa}_2\text{Cu}_3\text{O}_{7-\delta}$ . Within the MEL enhancement window the stiffness and pinning are both enhanced relative to a purely homogeneous superconducting background.

currents observed in YBCO.

#### D. Disorder, percolation, and loss of global coherence

As the disorder strength  $W$  increases, the spatial distributions of  $\rho_{\text{MEL}}$  and  $|\psi|$  become progressively more fragmented. At moderate  $W$ , superconducting regions connected via MEL-enhanced stiffness still percolate, and the system retains global phase coherence. Beyond a critical disorder threshold, the superconducting fraction drops below the percolation limit and global superconductivity is lost, even though sizable local  $|\psi|$  persists on isolated islands.

Figure 3 summarizes this percolation physics in terms of the domain continuity fraction  $f_c$  and a normalized local conductance proxy  $G(x)$ . For weak disorder,  $f_c \approx 1$  and MEL active superconducting paths percolate across the sample. As  $\sigma/A_0$  is increased,  $f_c$  drops sharply once the percolation threshold is crossed, in parallel with a rapid change in  $G(x)$  as a function of oxygen content. The MEL enhancement window occupies the relatively clean side of this diagram, where disorder is strong enough to generate an inhomogeneous landscape but not so strong as to destroy connectivity. This picture is qualitatively consistent with experimental observations that moderate disorder can leave  $T_c$  and superfluid density relatively robust, whereas strong disorder eventually suppresses global superconductivity via fragmentation of current paths.<sup>[2]</sup>

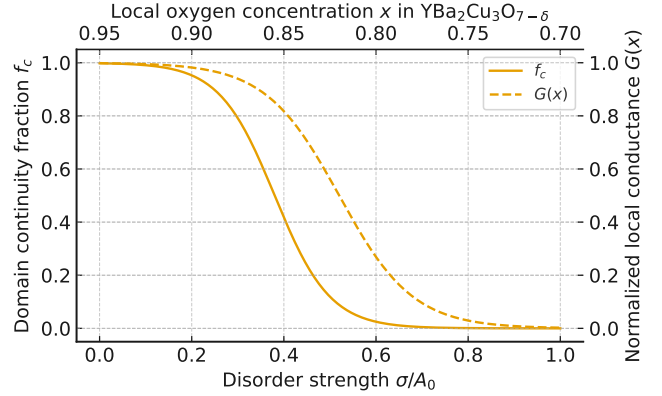


FIG. 3. Percolation of MEL active domains under disorder and its connection to oxygen stoichiometry. The lower horizontal axis shows the dimensionless disorder strength  $\sigma/A_0$ , defined as the ratio of the standard deviation of the local MEL amplitude to its clean-limit scale. The left vertical axis (solid curve) gives the domain continuity fraction  $f_c$ , i.e. the fraction of the system participating in a system-spanning MEL enhanced superconducting network. For weak disorder  $f_c \approx 1$ , while above a threshold  $\sigma/A_0 \sim 0.3$ – $0.4$  the connectivity collapses rapidly, signaling a percolation driven loss of global phase stiffness. The upper horizontal axis indicates a representative mapping to local oxygen concentration  $x$  in  $\text{YBa}_2\text{Cu}_3\text{O}_{7-\delta}$ , and the right vertical axis (dashed curve) shows the corresponding MEL domain formation probability or normalized local conductance,  $G(x)$ , extracted from the same simulations. The coincidence of the sharp drop in  $f_c$  with the rapid change in  $G(x)$  highlights that MEL enhanced superfluid stiffness is controlled by the connectivity of MEL domains rather than by local order parameter amplitude alone.

#### E. Pseudogap phenomenology within MEL

The pseudogap regime in cuprates remains a subject of intense debate.<sup>[1–3]</sup> Within the MEL framework, we interpret the pseudogap as a regime where short-range, partially coherent MEL correlations have formed but global superconducting phase coherence is absent or fragile. In this regime  $\rho_{\text{MEL}}$  develops substantial amplitude and  $\xi_{\text{MEL}}$  grows, while  $|\psi|$  remains small on average or is strongly fluctuating. The local density of states exhibits a partial suppression at the Fermi level with  $q^*$ -modulated features in Fourier space, consistent with STM/STS observations of checkerboard or stripe like patterns in the pseudogap state of Bi-based cuprates.<sup>[6, 11, 12]</sup>

Once  $T_c$  is crossed, superconducting coherence develops and MEL becomes coherence linked via the couplings in Eq. (5). The  $q^*$  peak in the Fourier-transformed LDOS is predicted to sharpen and gain spectral weight as the condensate forms, in contrast to the weakening of static CDW order seen in resonant x-ray scattering below  $T_c$  in YBCO.<sup>[8, 9]</sup> This interpretation of the pseudogap is model dependent and not unique; PDW based

and other intertwined-order frameworks provide alternative explanations.[3, 20] The distinctive feature of MEL is the explicit short-range, coherence linked modulation tied to the  $d$ -wave condensate.

## V. MEL SPECIFIC EXPERIMENTAL SIGNATURES

The MEL framework gains credibility only if it produces specific, falsifiable predictions that differ from those of conventional CDW or PDW scenarios. In this section we highlight the most decisive signatures and their experimental prioritization.

### A. Temperature evolution of the $q^*$ peak across $T_c$

The first and most direct MEL signature is the temperature evolution of the  $q^*$  peak in Fourier transformed STS maps. In Bi-2212 and related systems, STM/STS experiments already reveal bond-centered modulations with wave vectors near  $q \approx 0.3$  in both the pseudogap and superconducting states.[6, 10–12] The MEL framework predicts a specific pattern for how the amplitude and width of this peak should evolve upon cooling through  $T_c$ .

In the pseudogap regime above  $T_c$ , short-range MEL correlations produce a finite but relatively broad  $q^*$  peak. As the temperature decreases toward  $T_c$ , both the amplitude and the correlation length of MEL grow, sharpening the peak. Once superconductivity sets in, the coherence-linked coupling amplifies regions where both  $\rho_{\text{MEL}}$  and  $|\psi|$  are large, leading to a further increase in the spectral weight at  $q^*$ . In other words, the  $q^*$  peak should either remain robust or become stronger as the system enters the superconducting state.

This behavior contrasts with standard static CDW competition scenarios, in which the development of superconductivity depletes the CDW order parameter and suppresses the x-ray intensity at the CDW wave vector.[8, 9] While one must be careful in comparing LDOS-based and x-ray-based signals, a systematic sharpening and strengthening of the  $q^*$  STS peak below  $T_c$  would be highly suggestive of a coherence linked modulation rather than a purely competing CDW.

Figure 4 depicts this predicted evolution schematically. The first phase of MEL testing in STM/STS should focus on Bi-based cuprates where high resolution LDOS maps are already routinely obtained.[6] The goal is to track the  $q^*$  peak as a function of  $T$  across  $T_c$  and to compare the results with the MEL expectation.

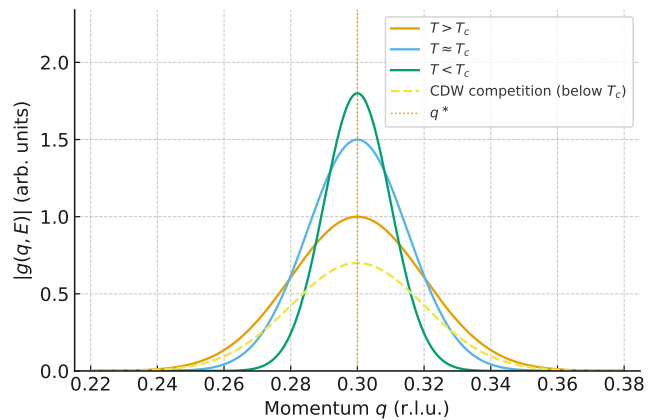


FIG. 4. Schematic Fourier transform STS intensity  $|g(q, E)|$  near the bond direction wave vector  $q^* \simeq 0.3$  r.l.u. across the superconducting transition. Solid curves show the MEL scenario: above  $T_c$  ( $T > T_c$ ) the  $q^*$  peak is broad and relatively weak, at  $T \approx T_c$  it is moderately enhanced, and below  $T_c$  ( $T < T_c$ ) it becomes both sharper and higher in intensity as the MEL envelope  $\Phi(\mathbf{r})$  locks to the superconducting condensate  $\psi(\mathbf{r})$ . The vertical dotted line marks  $q^*$ . For comparison, the dashed curve sketches a conventional CDW competition scenario in which the  $q^*$  peak is reduced below  $T_c$  as the competing superconducting gap opens. The qualitative trend in the  $q^*$  peak height and width across  $T_c$  provides a decisive discriminator between MEL and pure CDW competition.

### B. Local gap modulation correlation $\Delta(\mathbf{r})$ vs. $\rho_{\text{MEL}}(\mathbf{r})$

The second decisive MEL signature is the spatial correlation between the local superconducting gap magnitude  $\Delta(\mathbf{r})$  and the local MEL amplitude, which we denote here as a proxy for  $\rho_{\text{MEL}}(\mathbf{r})$ . In STM/STS studies,  $\Delta(\mathbf{r})$  is extracted from the energy position of coherence peaks or from a suitable LDOS criterion, while the modulation amplitude can be characterized by the local Fourier amplitude at  $q^*$  or by filtering the real-space data.

Within MEL, coherence linked couplings ensure that the preferred charge-modulation amplitude grows with the local superconducting coherence. Consequently, we predict a positive spatial correlation between the superconducting gap  $\Delta(\mathbf{r})$  and the MEL amplitude  $\rho_{\text{MEL}}(\mathbf{r})$ , quantified by a coefficient  $C_{\Delta, \text{MEL}} > 0$ . This trend is fundamentally different from conventional CDW scenarios, where charge order domains typically anticorrelate with the gap. In MEL the correlation persists over a broad temperature window below  $T_c$  and becomes strongest in the enhancement regime, providing a direct and falsifiable STM/STS signature. Regions exhibiting stronger  $q^*$  modulation should therefore display larger  $\Delta(\mathbf{r})$  on average, a prediction that can be tested by comparing gap maps with Fourier-filtered LDOS maps at  $q^*$ .

By contrast, in conventional CDW competition scenarios a strong modulation tends to suppress the superconducting order parameter, leading to an anti cor-



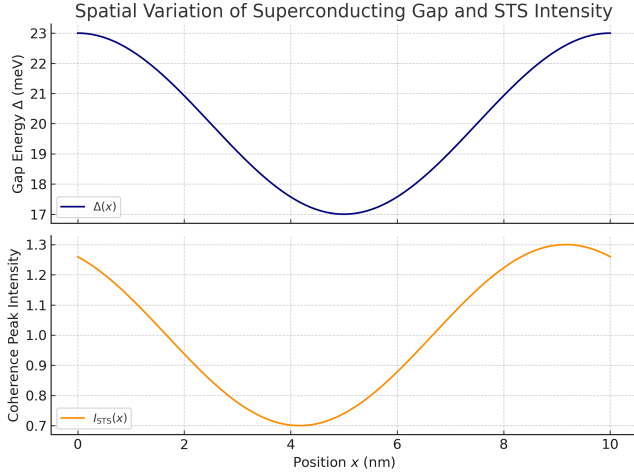


FIG. 5. Real space correlation between the local superconducting gap and MEL related modulation strength. The upper panel shows the simulated gap magnitude  $\Delta(x)$  along a one-dimensional cut through the sample, and the lower panel shows the corresponding Fourier transform STS coherence peak intensity or local MEL amplitude along the same cut. Regions with larger  $\Delta(x)$  coincide with stronger modulation, demonstrating the positive spatial correlation characteristic of a coherence linked MEL state. Such a trend is difficult to reconcile with simple CDW competition scenarios, which typically produce anti correlation between charge order and superconducting gap strength.

relation between  $\Delta(\mathbf{r})$  and the charge modulations.[3, 9] PDW-based scenarios can in principle produce more complex patterns, including sign changes and nodes in the pair amplitude, but a robust positive correlation between  $\Delta(\mathbf{r})$  and a predominantly charge-like modulation is not generic.[20]

Figure 5 illustrates the MEL expectation. Quantitatively, one can define a correlation coefficient  $C_{\Delta, \text{MEL}}$  between the local gap and the local modulation amplitude and measure it as a function of temperature and doping. A positive  $C_{\Delta, \text{MEL}}$  that strengthens below  $T_c$  would strongly support the MEL interpretation.

### C. Correlation length $\xi_{\text{MEL}}(T, W)$ and disorder effects

A third MEL related observable is the evolution of the MEL correlation length  $\xi_{\text{MEL}}$  with temperature and disorder. In STS experiments,  $\xi_{\text{MEL}}$  can be extracted from the real-space autocorrelation of the filtered  $q^*$  component or from the width of the  $q^*$  peak in Fourier space. In x-ray scattering, line widths of charge order peaks provide a complementary measure.

Within the GL framework,  $\xi_{\text{MEL}}$  grows upon cooling from  $T^*$  toward  $T_c$ , reflecting the increasing strength of short range MEL correlations, and then saturates or modestly increases further below  $T_c$  as coherence linked

effects become important. Disorder reduces  $\xi_{\text{MEL}}$  by breaking up domains and can ultimately suppress MEL altogether once the percolation threshold is crossed. The dependence of  $\xi_{\text{MEL}}(T, W)$ , together with measurements of  $\lambda_{ab}(T, W)$  and  $J_c(W)$ , offers a way to test whether the enhancement window in Table I is realized in a given material.

### D. Percolation behavior and oxygen disorder

The percolation-like loss of global superconductivity with increasing disorder, discussed in Sec. IV, suggests experiments where controlled disorder is introduced through oxygen ordering, ion irradiation, or chemical substitution. In YBCO, varying oxygen content and ordering in the Cu-O chains modifies both the hole concentration and the disorder landscape. Within the MEL picture one expects a regime where changes in chain oxygen ordering primarily rearrange the stiffness landscape and MEL domains without drastically altering the mean hole concentration. In such a regime the superfluid density and  $T_c$  may remain relatively robust until disorder induced fragmentation reaches the percolation threshold, at which point both quantities collapse rapidly.

Mapping this behavior as a function of oxygen ordering and comparing it with independent measures of charge correlations would provide a stringent test of MEL. Similar reasoning applies to controlled irradiation experiments, where disorder can be tuned at fixed composition.

### E. Experimental prioritization: Bi-based systems vs. YBCO

From a practical standpoint, early MEL testing should focus on materials where high resolution STM/STS is well established and where orthorhombic complications are minimal. Bi-2212 and related Bi-based cuprates are therefore natural first targets.[6, 10–12] In these materials the two most decisive and relatively unambiguous MEL signatures are the temperature evolution of the  $q^*$  peak across  $T_c$  and the local  $\Delta(\mathbf{r})$  versus modulation amplitude correlation. Both can be probed with existing STM/STS techniques.

YBCO, with its Cu-O chains and orthorhombic lattice, offers additional opportunities to test MEL via anisotropic responses along the  $a$  and  $b$  axes. However, such experiments are more challenging due to surface preparation and cleaving issues. We therefore view detailed  $a/b$ -anisotropy studies in YBCO as a second phase program to be pursued once the Bi-based STM/STS signatures are established. In this second phase, the anisotropic GL coefficients  $K_{s,x}$ ,  $K_{s,y}$ ,  $K_{\rho,x}$ ,  $K_{\rho,y}$ , and possibly anisotropic couplings  $\gamma_{1,2}$  can be constrained by measurements of directional stiffness, vortex behavior, and charge correlations.

## VI. RELATION TO INTERTWINED ORDERS AND LIMITATIONS

The MEL framework should be placed in the broader context of intertwined orders in cuprates.[2, 3, 20] Static long-range CDW, as detected by resonant x-ray scattering in YBCO and related compounds, is well established as a competitor to superconductivity. PDW states, in which the superconducting order parameter itself is spatially modulated, provide another route to intertwined charge and superconducting orders. Nematic and spin orders further enrich the landscape.

MEL can be viewed as a phenomenological coarse graining of a subset of these intertwined tendencies, focusing on a short range charge modulation at  $q^*$  that becomes energetically favored in the presence of  $d$  wave superconducting coherence. It does not preclude more microscopic PDW physics or other intertwined orders; indeed, in some microscopic realizations a PDW might generate an effective MEL sector at longer length scales. The distinguishing feature of MEL is its explicit treatment as a separate charge sector field  $\rho_{\text{MEL}}$  with a preferred  $q^*$ , coupled to but not identical with the superconducting order parameter.

Several limitations of the present work should be highlighted. First, the GL functional is classical and does not include quantum fluctuations, which can be important in underdoped regimes and near quantum critical points. Second, nodal quasiparticles and strong-coupling effects are not explicitly treated. These effects are known to influence the temperature dependence of the superfluid stiffness and to modify the response to disorder.[19] Third, the parameterization of  $\alpha(q)$  is phenomenological; while it reflects the observed anomalies in  $\chi_{\text{el}}(q)$  and bond stretching phonons, it is not derived from a microscopic Hamiltonian. Fourth, the present simulations focus on near optimally doped YBCO and do not attempt a systematic survey across the full doping phase diagram.

Given these limitations, the MEL framework should be regarded as an internally consistent, experiment constrained GL construction that organizes a range of observations and yields concrete predictions, rather than as a complete theory of high- $T_c$  superconductivity. Its most specific and falsifiable predictions concern the behavior of  $q^*$  modulations and their correlations with the superconducting gap and stiffness. Confirmation or falsification of these predictions will help to clarify whether MEL captures an essential aspect of the cuprate phenomenology or whether the dominant intertwined orders are better described by alternative frameworks.

## VII. OUTLOOK: BDG PROGRAM AND MICROSCOPIC EXTENSIONS

A central next step is a fully microscopic treatment of MEL within a self consistent BdG framework. The BdG

program underway proceeds along several lines. First, the electronic band structure of a representative cuprate (initially YBCO or Bi-2212) is combined with a  $d$ -wave pairing interaction and a periodic potential representing a modulation at  $q^* \approx 0.3$  along the bond directions. Second, self consistent solutions are obtained for the BdG equations in the presence of this modulation, yielding reconstructed bands, LDOS maps, and current-current correlation functions. Third, the microscopic superfluid stiffness is computed from the current-current response and compared with the corresponding GL-level stiffness, thereby testing the working hypothesis that short-range MEL can produce a modest stiffness enhancement. Finally, the BdG solutions may reveal whether a preferred  $q^*$  emerges dynamically from the interplay of electronic interactions and phonons, thereby providing a microscopic underpinning for the phenomenological  $\alpha(q)$ .

In parallel, first principles and density functional based studies of  $\chi_{\text{el}}(q)$  and bond-stretching phonons in cuprates can refine the parameterization of  $\alpha(q)$ . Existing inelastic x-ray and neutron data already indicate anomalies near  $q \approx 0.3$  in YBCO and related compounds,[13, 14] but a quantitative mapping from these anomalies to the effective GL coefficients remains to be completed.

On the experimental side, the near term priority is to carry out the STM/STS measurements required to test the MEL specific signatures in Bi-based cuprates. This includes high-resolution temperature dependent Fourier mappings of the LDOS near  $q^*$  across  $T_c$ , detailed studies of the local  $\Delta(\mathbf{r})$  versus modulation amplitude correlation, and measurements of the MEL correlation length as a function of temperature and disorder. Complementary muon spin rotation and microwave experiments can track  $\lambda_{ab}(T)$  and its dependence on disorder and strain in samples where MEL signatures are established.

Looking further ahead, once the MEL signatures are either confirmed or ruled out in Bi-based systems, the anisotropic physics of YBCO provides a rich arena for more refined tests. Direction-dependent stiffness measurements, vortex imaging along different crystallographic directions, and directional charge order studies by x-ray scattering can be combined with the anisotropic GL and BdG frameworks to explore how MEL couples to chain bands and orthorhombicity.

Ultimately, the MEL framework should be judged by its ability to connect microscopic modeling, GL phenomenology, and experimental observables in a coherent way. The present work provides the GL foundation and delineates the key predictions. The forthcoming BdG calculations and STM/STS campaigns will determine whether MEL is a useful organizing principle for cuprate superconductivity or whether the field must turn to alternative intertwined-order scenarios.

## Appendix A: Phenomenological parameterization of $\alpha(q)$ and selection of $q^*$

For completeness we collect a slightly more explicit parameterization of the momentum dependent coefficient  $\alpha(q)$  entering the MEL sector. Motivated by inelastic x-ray and neutron scattering data in YBCO and related cuprates,[9, 13, 14] we take

$$\alpha(q) = \alpha_0 + c_{\text{el}}\chi_{\text{el}}(q) + c_{\text{ph}}D_{\text{ph}}(q), \quad (\text{A1})$$

where  $\chi_{\text{el}}(q)$  is a coarse-grained electronic charge susceptibility and  $D_{\text{ph}}(q)$  represents the dispersion of the relevant bond stretching phonon branches. A simple illustrative form is

$$\begin{aligned} \chi_{\text{el}}(q) &= \frac{\chi_0}{1 + \xi_\chi^2(q - q_\chi)^2}, \\ D_{\text{ph}}(q) &= \frac{D_0}{\Omega(q)}, \end{aligned} \quad (\text{A2})$$

where  $q$  denotes the magnitude of the in-plane wave vector along a Cu–O bond direction,  $\xi_\chi$  is an electronic correlation length,  $q_\chi$  is the wave vector at which the electronic susceptibility peaks, and  $\Omega(q)$  is the bond stretching phonon frequency. Both  $\chi_{\text{el}}(q)$  and  $D_{\text{ph}}(q)$  are enhanced near  $q \approx 0.3$  in reciprocal lattice units, so that the combined  $\alpha(q)$  in Eq. (A1) develops a minimum at

$$q^* \approx \arg \min_q [\alpha_0 + c_{\text{el}}\chi_{\text{el}}(q) + c_{\text{ph}}D_{\text{ph}}(q)]. \quad (\text{A3})$$

In practice we treat  $q^*$  as fixed by experiment, but the above form makes explicit that it follows from a competition between electronic and phononic contributions rather than being inserted by hand.

The curvature of  $\alpha(q)$  at  $q^*$  sets an effective stiffness in momentum space that controls the spread of  $\rho_{\text{MEL}}(q)$  around  $q^*$  and hence the real-space correlation length  $\xi_{\text{MEL}}$ . Within GL simulations, the combination of parameters is chosen such that  $\xi_{\text{MEL}}$  lies in the 10–30 lattice-spacing range in the enhancement window (Table I), consistent with short-range but nontrivial coherence.

## Appendix B: Outline of the MEL Bogoliubov–de Gennes program

The BdG program sketched in Sec. VII proceeds from a minimal microscopic model designed to capture the essential physics of MEL at the quasiparticle level. One convenient choice is a two dimensional tight-binding Hamiltonian on a square lattice representing the  $\text{CuO}_2$  planes,

$$H_0 = \sum_{\mathbf{k}, \sigma} \epsilon_{\mathbf{k}} c_{\mathbf{k}\sigma}^\dagger c_{\mathbf{k}\sigma}, \quad (\text{B1})$$

with dispersion

$$\begin{aligned} \epsilon_{\mathbf{k}} &= -2t(\cos k_x + \cos k_y) - 4t' \cos k_x \cos k_y \\ &\quad - 2t''(\cos 2k_x + \cos 2k_y) - \mu, \end{aligned} \quad (\text{B2})$$

where  $(t, t', t'')$  are hopping parameters chosen to reproduce a representative cuprate Fermi surface and  $\mu$  fixes the doping.

A  $d$ -wave pairing interaction is then introduced at the mean field level,

$$H_\Delta = \sum_{\mathbf{k}} \left[ \Delta_{\mathbf{k}} c_{\mathbf{k}\uparrow}^\dagger c_{-\mathbf{k}\downarrow}^\dagger + \text{H.c.} \right], \quad \Delta_{\mathbf{k}} = \Delta_0 \frac{\cos k_x - \cos k_y}{2}, \quad (\text{B3})$$

together with a periodic potential representing MEL,

$$H_{\text{MEL}} = V_q \sum_{\mathbf{r}, \sigma} \cos(\mathbf{q}^* \cdot \mathbf{r}) c_{\mathbf{r}\sigma}^\dagger c_{\mathbf{r}\sigma}, \quad (\text{B4})$$

with  $\mathbf{q}^*$  along a Cu–O bond direction and  $V_q$  setting the modulation amplitude. The full BdG Hamiltonian  $H = H_0 + H_\Delta + H_{\text{MEL}}$  is then diagonalized in real space on finite clusters with periodic boundary conditions, and the pairing field  $\Delta_{\mathbf{r}}$  is updated self-consistently.

From the converged BdG solutions one can compute the reconstructed band structure, the LDOS  $N(\mathbf{r}, E)$ , and the current–current correlation function entering the microscopic superfluid stiffness. The effect of  $H_{\text{MEL}}$  on nodal and antinodal quasiparticles, on the superfluid density, and on the real space patterns in  $N(\mathbf{r}, E)$  can then be directly compared with both the GL level expectations and STM/STS data. In particular, one can test whether a modest positive correction to the stiffness of order ten percent survives in the presence of realistic nodal quasiparticles and Fermi surface reconstruction, or whether the net effect is neutral or negative. This comparison will provide a quantitative check on the GL-level working hypothesis that short-range MEL can enhance the phase stiffness in an experimentally relevant window.

## Appendix C: Example MEL real-space configuration

For completeness we show in Fig. 6 a representative real-space snapshot of the MEL field  $\rho_{\text{MEL}}(\mathbf{r})$  used in the GL and TDGL simulations. The configuration is generated by sampling the MEL sector of the free energy in the regime where the quadratic coefficient  $\alpha(\mathbf{q})$  is minimized on a ring at  $|\mathbf{q}| \simeq q^* \approx 0.3$  r.l.u. and the correlation length satisfies  $\xi_{\text{MEL}} \gtrsim 10\text{--}15 a_0$ . The resulting pattern consists of short-range, stripe like modulations along a Cu–O bond direction with a well-defined local phase that varies slowly on the scale of the lattice but is not globally ordered. This illustrates the defining features of MEL: the modulation is short range and partially coherent, forming domains of typical size  $\xi_{\text{MEL}}$ , and is thus distinct from a long-range static CDW. When coupled to the superconducting order parameter via  $F_{\text{cpl}}$ , the phase of these domains tends to lock to the condensate phase, leading to the coherence-linked enhancement of superfluid stiffness discussed in the main text.

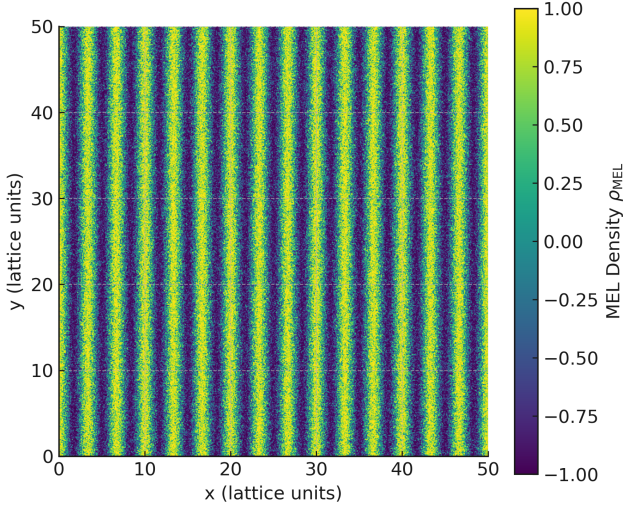


FIG. 6. Example real-space configuration of the MEL density field  $\rho_{\text{MEL}}(\mathbf{r})$  on a  $50 \times 50$  lattice. Colors represent the local value of  $\rho_{\text{MEL}}$  in arbitrary units. The pattern consists of short-range, stripe-like modulations along a Cu–O bond direction with correlation length  $\xi_{\text{MEL}}$  of order 10–15 lattice spacings and a spatially varying local phase. Such configurations are typical in the MEL enhancement window where the quadratic coefficient  $\alpha(\mathbf{q})$  is minimized at  $|\mathbf{q}| \approx q^* \simeq 0.3 \text{ r.l.u.}$  but long-range CDW order has not formed.

## ACKNOWLEDGMENTS

We are grateful to colleagues involved in the experimental MEL program for extensive discussions and for sharing insights from ongoing STM/STS and x-ray work. Internal MEL reports and technical notes have been invaluable in shaping the present GL formulation. D.A.R. and W.K. acknowledge support and facilities provided by the University of California, Berkeley.

- 
- [1] T. Timusk and B. Statt, “The pseudogap in high-temperature superconductors: An experimental survey,” *Rep. Prog. Phys.* **62**, 61 (1999).
  - [2] B. Keimer, S. A. Kivelson, M. R. Norman, S. Uchida, and J. Zaanen, “From quantum matter to high-temperature superconductivity in copper oxides,” *Nature* **518**, 179 (2015).
  - [3] E. Fradkin, S. A. Kivelson, and J. M. Tranquada, “Theory of intertwined orders in high temperature superconductors,” *Rev. Mod. Phys.* **87**, 457 (2015).
  - [4] A. Damascelli, Z. Hussain, and Z.-X. Shen, “Angle-resolved photoemission studies of the cuprate superconductors,” *Rev. Mod. Phys.* **75**, 473 (2003).
  - [5] M. R. Norman, H. Ding, M. Randeria *et al.*, “Destruction of the Fermi surface in underdoped high- $T_c$  superconductors,” *Nature* **392**, 157 (1998).
  - [6] Ø. Fischer, M. Kugler, I. Maggio-Aprile, C. Berthod, and C. Renner, “Scanning tunneling spectroscopy of high-temperature superconductors,” *Rev. Mod. Phys.* **79**, 353 (2007).
  - [7] G. Ghiringhelli *et al.*, “Long-range incommensurate charge fluctuations in  $(\text{Y,Nd})\text{Ba}_2\text{Cu}_3\text{O}_{6+x}$ ,” *Science* **337**, 821 (2012).
  - [8] J. Chang *et al.*, “Direct observation of competition between superconductivity and charge density wave order in  $\text{YBa}_2\text{Cu}_3\text{O}_{6.67}$ ,” *Nat. Phys.* **8**, 871 (2012).
  - [9] R. Comin and A. Damascelli, “Resonant x-ray scattering studies of charge order in cuprates,” *Annu. Rev. Condens. Matter Phys.* **7**, 369 (2016).
  - [10] J. E. Hoffman *et al.*, “A four unit cell periodic pattern of quasi-particle states surrounding vortex cores in  $\text{Bi}_2\text{Sr}_2\text{CaCu}_2\text{O}_{8+\delta}$ ,” *Science* **295**, 466 (2002).
  - [11] M. Vershinin, S. Misra, S. Ono, Y. Abe, Y. Ando, and A. Yazdani, “Local ordering in the pseudogap state of the high- $T_c$  superconductor  $\text{Bi}_2\text{Sr}_2\text{CaCu}_2\text{O}_{8+\delta}$ ,” *Science* **303**, 1995 (2004).
  - [12] W. D. Wise *et al.*, “Charge-density-wave origin of cuprate checkerboard visualized by scanning tunnelling microscopy,” *Nat. Phys.* **4**, 696 (2008).
  - [13] D. Reznik, L. Pintschovius, M. Ito, S. Iikubo, M. Sato, H. Goka, M. Fujita, K. Yamada, G. D. Gu, and J. M. Tranquada, “Electron-phonon coupling reflecting dynamic charge inhomogeneity in copper oxide superconductors,” *Nature* **440**, 1170 (2006).
  - [14] M. Le Tacon *et al.*, “Inelastic x-ray scattering in  $\text{YBa}_2\text{Cu}_3\text{O}_{6.6}$  reveals giant phonon anomalies and elastic central peak due to charge-density-wave formation,” *Nat. Phys.* **10**, 52 (2014).
  - [15] J. E. Sonier *et al.*, “New muon-spin-rotation measurement of the temperature dependence of the magnetic penetration depth in  $\text{YBa}_2\text{Cu}_3\text{O}_{6.95}$ ,” *Phys. Rev. Lett.* **72**, 744 (1994).
  - [16] J. E. Sonier *et al.*, “Hole-doping dependence of the magnetic penetration depth and vortex core size in  $\text{YBa}_2\text{Cu}_3\text{O}_y$ : Evidence for stripe correlations near 1/8 hole doping,” *Phys. Rev. B* **76**, 134518 (2007).
  - [17] B. Pümpin *et al.*, “Muon-spin-rotation measurements of the London penetration depths in  $\text{YBa}_2\text{Cu}_3\text{O}_{6.97}$ ,” *Phys. Rev. B* **42**, 8019 (1990).



- [18] G. Blatter, M. V. Feigel'man, V. B. Geshkenbein, A. I. Larkin, and V. M. Vinokur, "Vortices in high-temperature superconductors," *Rev. Mod. Phys.* **66**, 1125 (1994).
- [19] J. F. Annett, *Superconductivity, Superfluids and Condensates* (Oxford University Press, Oxford, 2004).
- [20] D. F. Agterberg, J. C. S. Davis, S. D. Ekins, E. Fradkin, D. J. Van Harlingen, S. A. Kivelson, P. A. Lee, L. Radzihovsky, J. M. Tranquada, and Y. Wang, "The physics of pair-density waves: Cuprate superconductors and beyond," *Annu. Rev. Condens. Matter Phys.* **11**, 231 (2020).